Co-implantation of magnesium and zinc ions into titanium regulates the behaviors of human gingival fibroblasts

Lanyu Wang[a,b], Qiming Luo[a,b], Xianming Zhang[a], Jiajun Qiu[a], Shi Qian[a,c,*], Xuanyong Liu[a,b,c,d,**]

[a] *State Key Laboratory of High Performance Ceramics and Superfine Microstructure, Shanghai Institute of Ceramics, Chinese Academy of Sciences, Shanghai, 200050, China*
[b] *Center of Materials Science and Optoelectronics Engineering, University of Chinese Academy of Sciences, Beijing, 100049, China*
[c] *Cixi Center of Biomaterials Surface Engineering, Shanghai Institute of Ceramics, Chinese Academy of Sciences, Ningbo, 315300, China*
[d] *School of Chemistry and Materials Science, Hangzhou Institute for Advanced Study, University of Chinese Academy of Sciences, 1 Sub-lane Xiangshan, Hangzhou, 310024, China*

ARTICLE INFO

ABSTRACT

Soft tissue sealing around implants acts as a barrier between the alveolar bone and oral environment, protecting implants from the invasion of bacteria or external stimuli. In this work, magnesium (Mg) and zinc (Zn) are introduced into titanium by plasma immersed ion implantation technology, and their effects on the behaviors of human gingival fibroblasts (HGFs) as well as the underlying mechanisms are investigated. Surface characterization confirms Mg and Zn exist on the surface in metallic and oxidized states. Contact angle test suggests that surface wettability of titanium changes after ion implantation and thus influences protein adsorption of surfaces. *In vitro* studies disclose that HGFs on Mg ion-implanted samples exhibit better adhesion and migration while cells on Zn ion-implanted samples have higher proliferation rate and amounts. The results of immunofluorescence staining and real-time reverse-transcriptase polymerase chain reaction (RT-PCR) suggest that Mg mainly regulates the motility and adhesion of HGFs through activating the MAPK signal pathway whereas Zn influences HGFs proliferation by triggering the TGF-β signal pathway. The synergistic effect of Mg and Zn ions ensure that HGFs cultured on co-implanted samples possessed both high proliferation rate and motility, which are critical to soft tissue sealing of implants.

1. Introduction

Owing to excellent mechanical properties and superior biocompatibility, titanium and its alloys are widely used as clinical implants in oral orthopedic for edentulous patients [1–4]. Nevertheless, there are still some possibilities of implant failures due to poor osseointegration, susceptible to bacteria and weak integration with soft tissue [5–8]. Compared with researches in osteogenic and anti-bacterial properties, far less attention from scientists and clinicians has been paid to improving the soft tissue sealing abilities of titanium and its alloys for these years [9–15]. Actually, ideal soft tissue sealing, a firm connection

between implants and adjacent soft tissue through collagen fibers, plays a critical role in dental restoration by implanting, since it acts as a promising protective barrier from harmful oral environment, thus reducing the probability of bacterial invasion and inevitable marginal bone loss [16–18]. Without the protection of effective soft tissue sealing, periodontal pocket and bone resorption, followed by implants destruction, would occur due to the external stimuli [18–20]. Therefore, developing an efficient method to improve the ability of soft tissue sealing of biomaterials is significant in dental implantation.

To satisfy these demands, some attempts have been made to ameliorate the soft tissue sealing ability of implants. Chen et al. used

hyaluronic acid to regulate the migration and inflammation of human gingival fibroblasts (HGFs) [21]. Wang et al. suggested injectable-pla-telet-rich fibrin had potential in speeding tissue regeneration [22]. Abe et al. reported ascorbic acid regulated the expression of alkaline phosphatase (ALP) in HGFs [23]. It was also reported that magnesium (Mg) and zinc (Zn) are essential supplementary elements to promote wound healing and rehabilitation of patients for the clinical treatment of soft tissue injury [24–27]. Mg had good biocompatibility and osseointe-gration, and Zn showed excellent antibacterial ability and good osteo-genic activity [15,28–31]. However, fewer researchers paid attention to taking advantage of inorganic elements such as Mg and Zn to improve the soft tissue sealing ability of implants. Furthermore, how they functioned in local regions during the process of wound healing and soft tissue regeneration was still not clear enough, so the study of the me-chanisms was urgent [32–36]. Considering all above, we supposed that the combination of Mg and Zn might have great potential in developing a kind of biomaterials with good soft tissue integration ability, as well as the osteogenic activity and antibacterial ability. Therefore, plasma immersion ion implantation (PIII), an efficient and well-developed technology that can introduce nearly any elements to chemically modify the surface of biomaterials like titanium without much damage on their surface morphologies, was chosen to establish a model for understanding the mechanism of Mg and Zn on promoting soft tissue integration [31].

In this work, Mg and Zn were implanted separately and co-im-planted into titanium to provide the Mg and Zn local delivery platform. The possible functional mechanism of Mg and Zn in soft tissue sealing was investigated via *in vitro* culturing HGFs on the prepared samples.

2. Material and methods

2.1. Sample preparation

Commercial pure titanium plates with dimensions of 10 mm × 10 mm × 1 mm and 20 mm × 20 mm × 1 mm were che-mically etched for 5 min and three times with a solution of HF: HNO$_3$: H$_2$O with a volume ratio of 1 : 4: 5. After the plates were cleaned with ultrapure water and dried in the air, Mg and Zn were ion implanted into the pre-treated samples at −30 kV for 60 min. The samples were de-signed as Mg-Ti and Zn-Ti, respectively. Mg/Zn co-implantation was carried out simultaneously using pulsed Mg and Zn cathodic arc plasma sources, and the samples were represented as Mg&Zn-Ti. Detailed parameters of PIII were listed in Table S1.

2.2. Sample characterization

Surface morphologies of all the samples were examined by a scan-ning electron microscope (SEM, Hitachi S-4800, Japan). The chemical compositions and states of various samples were detected by X-ray photoelectron spectroscopy (XPS, PHI 5802, Physical Electronics Inc., Eden Prairie, MN, USA) with a Mg Kα (1253.6 eV) source.

2.3. Surface wettability

Surface wettability of all the samples was determined with a contact angle tester (Automatic Contact Angle Meter Model SL200B, Solon, China) and ultrapure water was chosen as the test liquid. Details can be found in our previous works [37,38].

2.4. Mg and Zn release

The PIII-treated titanium samples were immersed in saline (10 mL) for 1, 4, 7, 14, 21 days at 37 ˚C without stirring. The amounts of re-leased Mg and Zn ions were detected by an ICP-AES (Varian Liberty 150, USA). In specific, the saline used to immerse samples evaporated, dissociated, ionized and was excited under the excitation source to generate optical radiation. Then the obtained composite light was spectrally dispersed into spectrum and the wavelength as well as the intensity of the spectral lines was detected for analyzing the con-centration of released ions in the saline. Moreover, the standard curve was established by setting the standard solutions with concentration of 0.001 ppm, 0.01 ppm, 0.1 ppm, 1 ppm and 10 ppm. The R^2 was guaranteed to be greater than or equal to 0.9999 and the detection limit was 0.001 ppm.

2.5. Protein adsorption

Samples from each group were put into a 24-well plate and cleaned twice with ultrapure water, and then were immersed in bovine serum albumin (BSA, 1 mg mL^{-1}, 1 mL, Sigma Aldrich, USA) solution and incubated for 24 h at 37 ˚C. After that, phosphate buffer saline (PBS, 10 mM) was used to rinse all sample twice, and 2 wt% lauryl sodium sulfate was added to each well to elute the adsorbed BSA. The elution process was conducted under shaking for 2 h at 37 ˚C. The standard curve of BSA was acquired by standard solutions with concentration gradient. The eluents of samples and the BSA standard solutions were mixed separately with testing solutions of BCA Protein Assay Kit, and their absorbance under 560 nm was detected by an enzyme-labeling instrument (BIO TEK, ELX 800). The amount of BSA adsorbed on dif-ferent sample surfaces was analyzed by standard curve fitting.

2.6. In vitro biological evaluation

2.6.1. Cell culture

HGFs used in this work were the major cells in peri-implant soft tissue and played a critical role in soft tissue integration in the wound-healing process [39,40]. HGFs (ScienCell Research Laboratories, USA) were cultured with fibroblasts medium (FM, ScienCell Research La-boratories, USA) at 37 ˚C in an environment of 5% CO$_2$. HGFs were passaged every 2 days and passages 4–6 were used in the experiments. For the assessment of the early cell adhesion and cytoskeleton mor-phology, HGFs with a concentration of 2.0 × 10^4 cells mL^{-1} were seeded on the sample surfaces. To evaluate cell proliferation, mor-phology, cytotoxicity of various samples and immunofluorescence analysis of Col-I and FN, cells at a density of 3.0 × 10^4 cells mL^{-1} were seeded onto each sample. To investigate the cell migration ability, HGFs with a density of 5.0 × 10^4 cells mL^{-1} were seeded on sample surfaces. As for real-time reverse-transcriptase polymerase chain reaction (RT-PCR) analysis, cells were cultured on samples at a density of 1.0 × 10^5 cells mL^{-1}.

2.6.2. Cell adhesion

To investigate the early cell adhesion on different samples, 4', 6-diamidino-2-phenylindole (DAPI, Sigma, USA) and Rhodamine-phal-loidin (Sigma, USA) staining were carried out. At each culture time point (1, 4, and 24 h), the cells on various samples were washed with PBS twice and transferred into a new 24-well plate. Then, HGFs were fixed with 4% Para-formaldehyde solution (PFA) for 10 min, permea-bilized with Triton X-100 (0.1 v/v%) for 2 min and blocked by BSA (1 wt% in PBS, Sigma Aldrich, USA) for 20 min successively. Afterwards, the cells were stained with fluorescein Rhodamine-phal-loidin and DAPI for 1 h and 5 min, respectively. Confocal laser-scanning microscope (CLSM, LeicaSP8, Germany) was used to obtain fluores-cence photographs of all samples.

2.6.3. Wound healing assay

To investigate the cell migration ability, wound healing assay was performed. After the cells grew on samples for 2 days and reached confluence, wounds of the cell monolayers on sample surfaces were made with a plastic pipette. Then, the cells were cultured for another 6 h and 12 h in fresh FM. After predetermined culturing periods, the samples were rinsed with PBS twice, transferred to a new 24-well plate
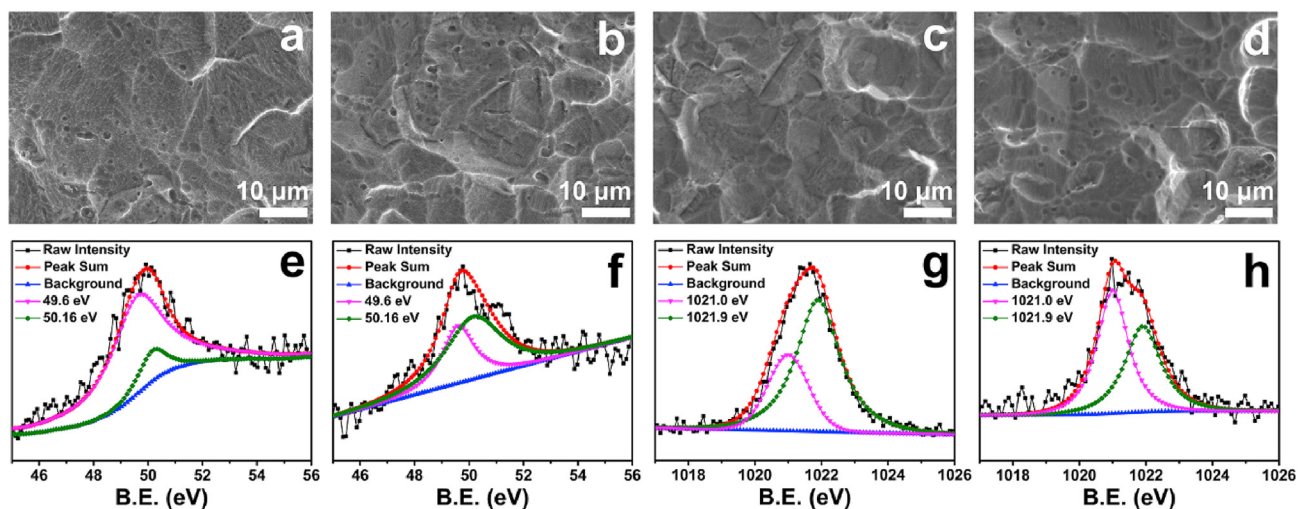
Fig. 1. Surface morphology of the acid etched titanium before and after ion implantation: (a) Ti, (b) Mg-Ti, (c) Zn-Ti, and (d) Mg Surface chemical composition and states analysis by XPS: (e) Mg 2p from Mg-Ti, (f) Mg 2p from Mg&Zn-Ti, (g) Zn 2p from Zn-Ti, and (h) Zn 2p from Mg&Zn-Ti.

and fixed with 4% PFA for 10 min at 4 °C. Then, HGFs were permeabilized with Triton X-100 (0.1 v/v%) for 2 min. After being blocked by BSA (1 wt%) for 20 min, fluorescein Rhodamine-phalloidin and DAPI were used for staining the HGFs for 1 h and 5 min, respectively. The fluorescence photographs of wounding regions on all samples were acquired with a CLSM. The statistical numbers of migrating HGFs were obtained by counting the cell nuclei in the wounding regions of three fluorescence-staining images of HGFs on samples in each group.

2.6.4. Cell live/dead staining

To assess the cytotoxicity of different samples, cell live/dead staining was conducted after the cells were cultured with samples for 3 days. At each culturing time point, the samples were rinsed with PBS twice and transferred into a new 24-well plate. After that, PBS (100 μL) with calcein-AM (0.1 μL) and propidium iodide (0.25 μL) was introduced to each sample and incubated for 15 min at 37 °C. After being rinsed twice with PBS, the fluorescent images of the cells were taken using a fluorescent microscope (Olympus, Japan).

2.6.5. Cell proliferation and morphology

Cell proliferation was evaluated using the alamarBlue™ method after the HGFs were cultured with various samples for 1, 3, and 5 days. Specifically, the samples were shifted into a new 24-well plate and gently rinsed with PBS twice at prescribed culturing time. Afterwards, fresh medium (0.5 mL) with 10% alamarBlue™ was added to each sample and incubated for another 2 h. After incubation, the fluorescent intensity of the cell culture medium (100 μL) was measured by a Microplate Reader at excitation wavelength of 560 nm and emission wavelength of 590 nm. For cell morphology observation, the samples with HGFs cultured for 3 days were fixed with 2.5% glutaraldehyde after each incubation time point. Then, gradient ethanol solutions (30, 50, 75, 90, 95, and 100 v/v%) and hexamethyldisilizane-ethanol solutions of different volume ratio was used sequentially to dehydrate the samples. Before SEM examination, the samples with HGFs were coated with platinum.

2.6.6. Immunofluorescence analysis of Col-I and FN

HGFs were cultured on the specimens for 1 and 3 days. At each time point, the cells were rinsed with PBS twice, fixed in 4% PFA for 30 min and blocked with BSA (1 wt%) for 30 min successively. Afterwards, HGFs were incubated overnight at 4 °C with primary antibody of anti-collagen I and anti-fibronectin (Abcam, UK), respectively. After being washed with PBS twice, the cells on samples were stained with fluorochrome-conjugated secondary antibody and DAPI sequentially. The

fluorescence photographs of the cells were observed using a CLSM. The semi-quantitative statistical analysis of immunofluorescence staining intensity reflecting Col-I secretion and FN accumulation were calculated by the area ratios of Col-I and FN to cell nucleus in fluorescent images using Image Pro Plus.

2.6.7. Quantitative RT-PCR analysis

RT-PCR was used to investigate the soft tissue sealing relative gene expression levels of HGFs cultured with various samples. Specifically, HGFs were seeded on all the samples for 7 days and during this period the culture medium was changed every there days. After prescribed culturing time, the HGFs were rinsed with PBS twice and the total RNA was extracted with TRIzol reagent (Invitrogen, Carlsbad, USA). After the RNA was purified with chloroform, isopropanol and 75% ethanol successively, the complementary DNA (cDNA) was reverse transcribed from the RNA (1 μg) using the Transcriptor First Strand cDNA Synthesis Kit (TaKaRa, Japan). The gene expression levels of Col-I, TGF-β, FN, Smad2, ITGB1, Smad3, MAPK3, ZIP7, Erk2 and ZIP13 were detected by the Roche LightCycler480 system with an SYBR Green I PCR Kit. All gene primers were synthesized rigorously (BioTNT Co., Ltd. Shanghai, China) and the detail information of all gene primers were listed in Table S2. Glyceraldehyde 3-phosphate dehydrogenase (GAPDH) was a reference gene to normalize all mRNA values.

2.7. Statistical analysis

All the data were expressed as the mean ± standard deviation (SD). The statistical analysis was carried out using a GraphPad Prism 5 software package. The statistical significant difference was measured by two-way analysis of variance and Tukey's multiple comparison tests and the value of $P < 0.05$ was considered statistically significant.

3. Results and discussion

3.1. Surface characterization

Surface morphologies of titanium before and after ion implantation were shown in SEM images (Fig. 1a-d). The rough acid-etched surface morphologies substantially were unchanged after ion implantation, suggesting that ion implantation did not damage the original microstructure of the materials and only formed a thin ions-containing film on their surfaces. The chemical composition and states were determined by XPS and the results were presented in Fig. 1e-h. The Mg 2p peaks at 50.16 eV and 49.6 eV obtained from Mg-Ti and Mg&Zn-Ti corresponded

Table 1
Atomic ratio of ion-implanted samples (%).

Samples	C 1s	O 1s	Ti 2p3	Mg 2p	Zn 2p
Mg-Ti	36.82	43.49	15.65	4.05	—
Zn-Ti	39.61	43.10	15.10	—	2.19
Mg&Zn-Ti	36.95	44.71	15.38	2.22	0.74

to oxidized and metallic Mg, respectively [15,28]. The Zn 2p peaks at 1021.9 eV and 1021.0 eV indicated the existence of oxidized and metallic Zn, respectively [28,31].

As shown in Table 1, the atomic ratio of various elements on sample surfaces confirmed the co-existence of Mg and Zn elements in co-implanted samples. The XPS spectra suggested that Mg and Zn both incorporated into titanium in the forms of metallic and oxidized state (Mg/MgO and Zn/ZnO). The concentration of Mg in Mg-Ti was more than that of Zn in Zn-Ti, which may be mainly due to easier ionization of Mg. The ionization energy E_Q was defined as energy required eliminating an electron from an isolated atom or an ion with charge Q. It can be expressed as Equation (1) [31]:

$$E_Q^{sum} = \sum_{Q'=0}^{Q-1} E_{Q'} \qquad 1$$

The ionization energy of Mg (7.64 eV) was less than that of Zn (9.39 eV) [31,41]. Therefore, the concentration of implanted Mg was more than that of Zn. Moreover, the concentration of implanted ions in co-implanted samples was slightly less than that of separately implanted samples. It may be due to the collisions between the Mg and Zn ions during co-implantation and subsequent energy loss.

Moreover, the water contact angles of all samples shown in Fig. 2a indicated that Mg ion implantation improved the hydrophilicity of titanium while Zn ion implantation increased its hydrophobicity. When Mg and Zn ions were co-implanted into the samples, their wettability increased, perhaps because when ZnO and MgO co-existed in the modified layers the hydrophobicity of ZnO film was improved by hydrophilic MgO [42–45].

The released kinetics of Mg and Zn ions in the ion-implanted titanium were studied by measuring the released Mg and Zn ions using an inductively coupled plasma atomic emission spectroscopy (ICP-AES). When the implanted samples were immersed in saline, chloridion and protons would dissolve implanted metals or their oxides on the substrate to form chloride and hydroxide with high solubility. Therefore, implanted elements would gradually release into saline with the extension of immersion time and the titanium substrate acted as a storage platform with implanted elements during the process of ions release. As shown in Fig. 2b, the concentration of Mg^{2+} leached from Mg&Zn-Ti was almost twice larger than that from Mg-Ti while Fig. 2c showed that the Zn^{2+} concentration of Zn-Ti was almost twice as much as that of Mg&Zn-Ti. However, the results of XPS (Table 1) suggested that the co-implanted sample surfaces had lower content of Mg and Zn compared with Mg-Ti or Zn-Ti. It was related to the difference between the standard electrode potential of Mg (− 2.372 V) and Zn (− 0.7618 V)

[46]. After the co-implanted samples were immersed in saline, the implanted Mg would serve as the anode instead of Zn since its lower standard electrode potential, and the following reaction (Equation (2)) would occur at the anode:

$$Mg \rightarrow Mg^{2+} + 2e^- \qquad 2$$

Meantime, the reaction that occurred at the cathode was shown as Equation (3).

$$2H^+ + 2e^- \rightarrow H_2 \qquad 3$$

Therefore, co-implanted samples released more Mg^{2+} than Mg-Ti and less Zn^{2+} than Zn-Ti due to the cathodic protection effect of Mg to Zn. It also explained that Mg^{2+} released from Mg&Zn-Ti almost reached the maximum after only one-day immersion while Mg^{2+} released from Mg-Ti lasted until Mg-Ti samples were immersed for 21 days. As for Zn^{2+} release, Mg&Zn-Ti exhibited lower Zn^{2+} release rate than Zn-Ti at first and higher release rate after 4-day immersion when Mg release in Mg&Zn-Ti reached plateau. Moreover, the total amount of released Zn^{2+} from Mg&Zn-Ti was lower than Zn-Ti, probably because Zn-Ti had higher amount of implanted ions than that of Mg&Zn-Ti (Table 1).

3.2. Protein adsorption

After the placement of biomedical implants in organisms, protein adsorption occurred first, a process important to adhesion, migration and proliferation of mammalian cell [47]. The amounts of adsorbed protein on various sample surfaces were presented in Fig. 3a. Mg-Ti and Mg&Zn-Ti adsorbed more protein than Zn-Ti and Ti. The result was consistent with the surface wettability of different samples. BSA preferred to be adsorbed on surface that was more hydrophilic when the contact angle of sample surface was lower than 100° [48–50].

3.3. Cell adhesion and migration assessment

HGFs were cultured on different samples to simulate peri-implant soft tissue sealing around the transmucosal area *in vitro*. The initial adhesion and spreading of HGFs had significant effects on subsequent cell activities such as cell migration [51,52]. The fluorescent images of HGFs were shown in Fig. 3b. HGFs on the ion-implanted samples exhibited better cell adhesion and spreading compared to Ti after being cultured for 1, 4, and 24 h. After 1 h incubation, cells on implanted samples had larger areas than those on Ti samples. After 4 h, HGFs on all samples began to spread and more filopodia extended outward, especially for Mg-Ti. After 24 h culturing, cells on Mg&Zn-Ti and Zn-Ti had similar density which was larger than on Ti and Mg-Ti, and the cells on Mg&Zn-Ti were somewhat more extended than on other groups of samples. The difference in adhesion and spreading of HGFs on various samples may be related to the different ions release, protein adsorption and surface hydrophilicity of various samples. From Fig. 2b and c, it was clear that Mg&Zn-Ti released Mg^{2+} faster and more than Mg-Ti and had almost the same release rate and amount of Zn^{2+} as Zn-Ti within the first day. It indicated that Mg^{2+} might be beneficial to HGFs
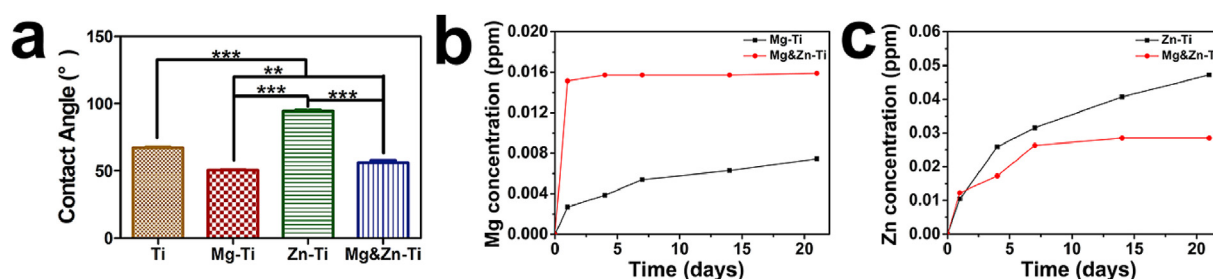
Fig. 2. Contact angles of water on different sample surfaces (*$p < 0.05$; **$p < 0.01$; ***$p < 0.001$) (a); Released Mg concentrations in saline after immersion for 1, 4, 7, 14, and 21 days (b); Released Zn concentrations in saline after immersion for 1, 4, 7, 14, and 21 days (c).
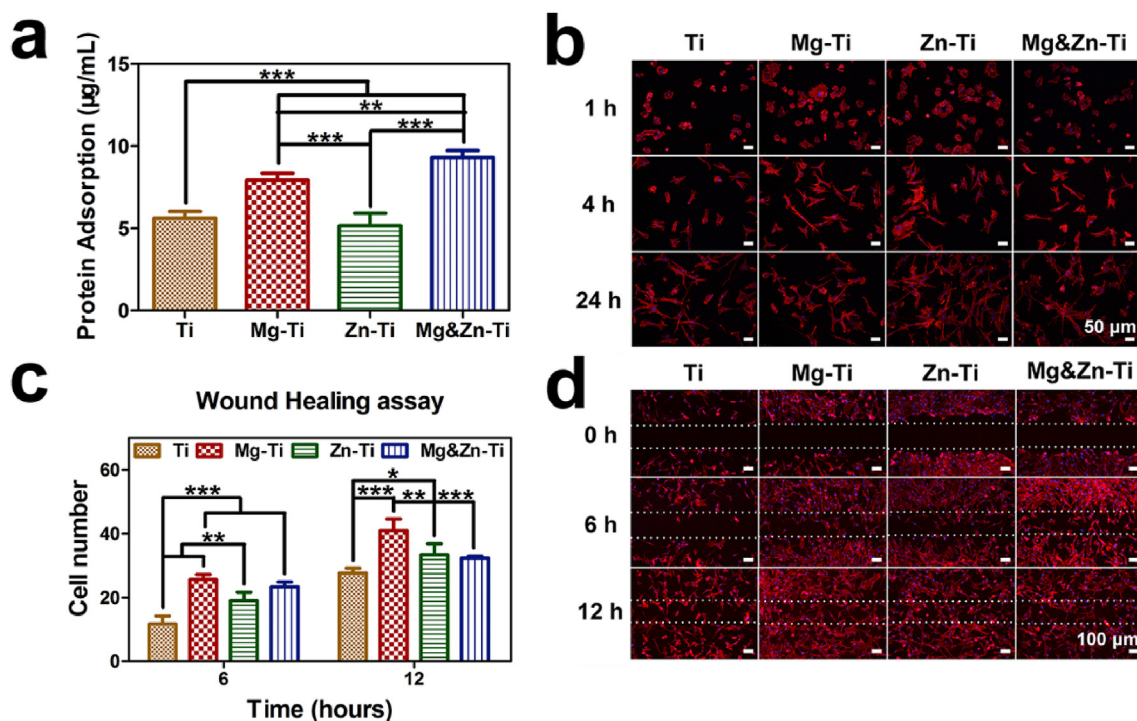
Fig. 3. Protein adsorption of BSA on various sample surfaces (a); Cell adhesion assay. Fluorescent images of HGFs cultured on different sample surfaces for 1, 4, and 24 h with actin stained with Rhodamine-phalloidin (red) and nuclei stained with DAPI (blue) (b); Numbers of HGFs in the wounding regions (c); CLSM images of the cytoskeleton stained HGFs on different samples in wound healing assay with actin stained with Rhodamine-phalloidin (red) and nuclei stained with DAPI (blue) (d); (*$p < 0.05$; **$p < 0.01$; ***$p < 0.001$).

adhesion and filopodia extension on sample surfaces at the early stage of culturing and Zn^{2+} at certain concentrations may mainly have effects on cell proliferation during the later stage after seeding. Mg-Ti and Mg&Zn-Ti can adsorb more proteins than Zn-Ti and Ti (Fig. 3a), which might be another reason for better cell adhesion on Mg ion-implanted samples. In addition, hydrophilicity also played a critical role in promoting cell adhesion on Mg-Ti than Mg&Zn-Ti at the very early stage of adhesion (Fig. 2a) [50].

The HGFs migration played an important role in soft tissue sealing after injury [53]. In order to investigate the migration ability of HGFs on various samples, wound healing assay was conducted. The fluorescent staining images and statistical cell numbers in wounding regions were presented in Fig. 3c and d, respectively. The migration ability of HGFs on all samples showed the following trend: Mg-Ti > Mg&Zn-Ti > Zn-Ti > Ti. Combined with the results of ions release (Fig. 2b and c), it implied that Mg^{2+} could promote the migration of HGFs while Zn^{2+} showed slightly positive function on cell migration. However, cells on Mg-Ti exhibited better migration ability than those on Mg&Zn-Ti. It was because even though Mg&Zn-Ti released more ions than Mg-Ti on the first day, its release rate of Mg^{2+} was lower than Mg-Ti after the first day. Therefore, the concentration of Mg^{2+} in the medium from Mg&Zn-Ti may be lower than that from Mg-Ti due to the change of culture medium during the wounding process after two-day culturing.

3.4. Cell vitality, proliferation and morphologies characterization

The cytotoxic assessment of various samples by live/dead staining was shown in Fig. 4a. None of the samples appeared to induce significant cell death which suggested all ion-implanted samples exhibited good cytocompatibility. Furtherore, the live HGFs on implanted samples were more than that on Ti samples. Although all ion-implanted samples exhibited good cytocompatibility, there were still a few dead cells on Zn-Ti compared with other samples, which may be due to the cytotoxicity of ZnO existing on the surface of Zn ion-implanted samples

[54,55]. Moreover, Mg&Zn-Ti showed less cytotoxicity than Zn-Ti owing to its lower content of implanted Zn ions and thus less ZnO on the surface (Table 1). In addition, the existence of Mg^{2+} in co-implanted samples may also reduce the adverse effects of ZnO to HGFs.

The results of alamarBlue™ assay in Fig. 4b also indicated that HGFs on ion-implanted samples had higher proliferation rate and vitality than those on Ti samples. Although there was no statistical difference on cell proliferation among all groups after 1 day, HGFs on ion-implanted samples were a little more than those on Ti samples on the third day. After 5 days, HGFs on ion-implanted samples showed obviously higher proliferation rates compared to those on Ti samples. It indicated that both Mg and Zn implantation could promote HGFs proliferation and growth. Combined with the results of cell adhesion, it can be proposed that Mg^{2+} had great effects on initial cell adhesion and there should be more cells on Mg-Ti than Zn-Ti due to cell growth with the extension of incubation time. However, the amount of HGFs on Zn-Ti was the highest among all groups. This result suggested Zn^{2+} probably played a major role in promoting HGFs proliferation when co-existed with Mg^{2+}. It can also prove that Mg&Zn-Ti had higher cell proliferation than Mg-Ti even though its release of Mg^{2+} was much smaller than Mg-Ti after the first day (Fig. 2b). Moreover, the release concentration of Zn^{2+} from Zn-Ti was more than from Mg&Zn-Ti, which may be the reason why HGFs on Zn-Ti showed slightly rapider growth than those on Mg&Zn-Ti.

Cell morphologies of HGFs cultured on various sample surfaces for 3 days were shown in Fig. 4c. It was consistent with the result of cell proliferation. There were more cells on Zn-Ti than other groups. HGFs on Zn-Ti had grown to reach confluence, completely covered the surfaces and a uniform layer of cells was formed.

3.5. Immunofluorescence analysis of Col-I and FN

Collagen (Col), a primary composition of extracellular matrix (ECM), plays an important role in the response of HGFs to the material
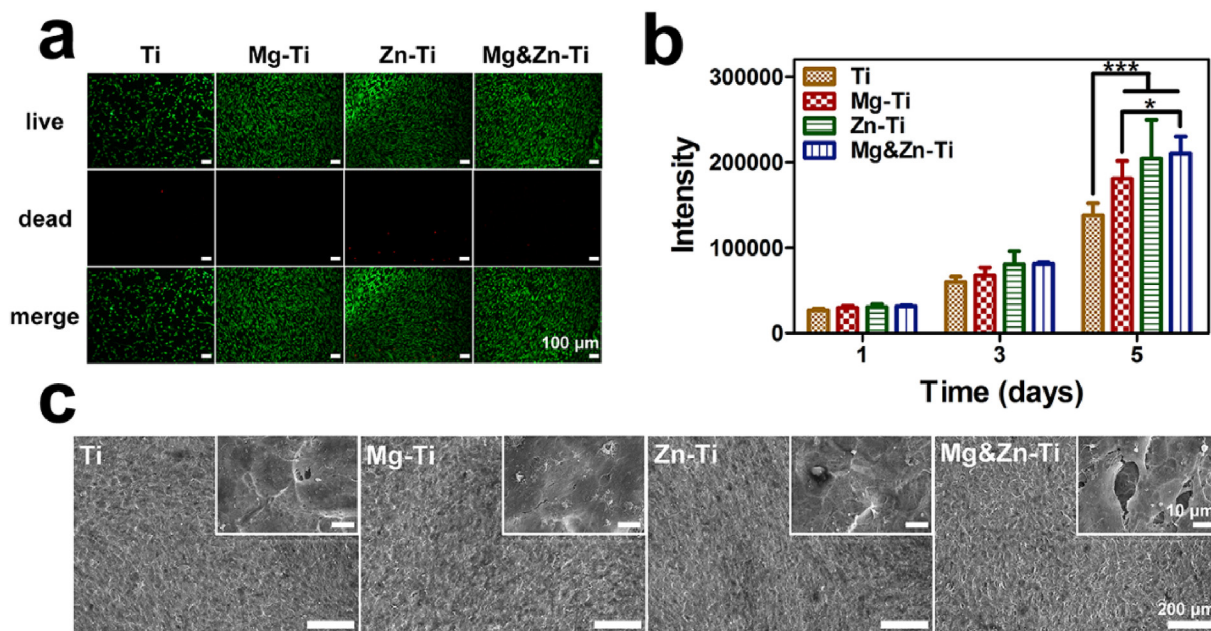
Fig. 4. Fluorescent images of HGFs on various samples with live cells stained with calcein-AM and dead cells stained with propidium iodide (a); HGFs proliferation activity on various sample surfaces were detected by alamarBlue™ for 1, 3, and 5 days (b); SEM morphology of HGFs cultured on various sample surfaces for 3 days (c); (*p < 0.05; **p < 0.01; ***p < 0.001).
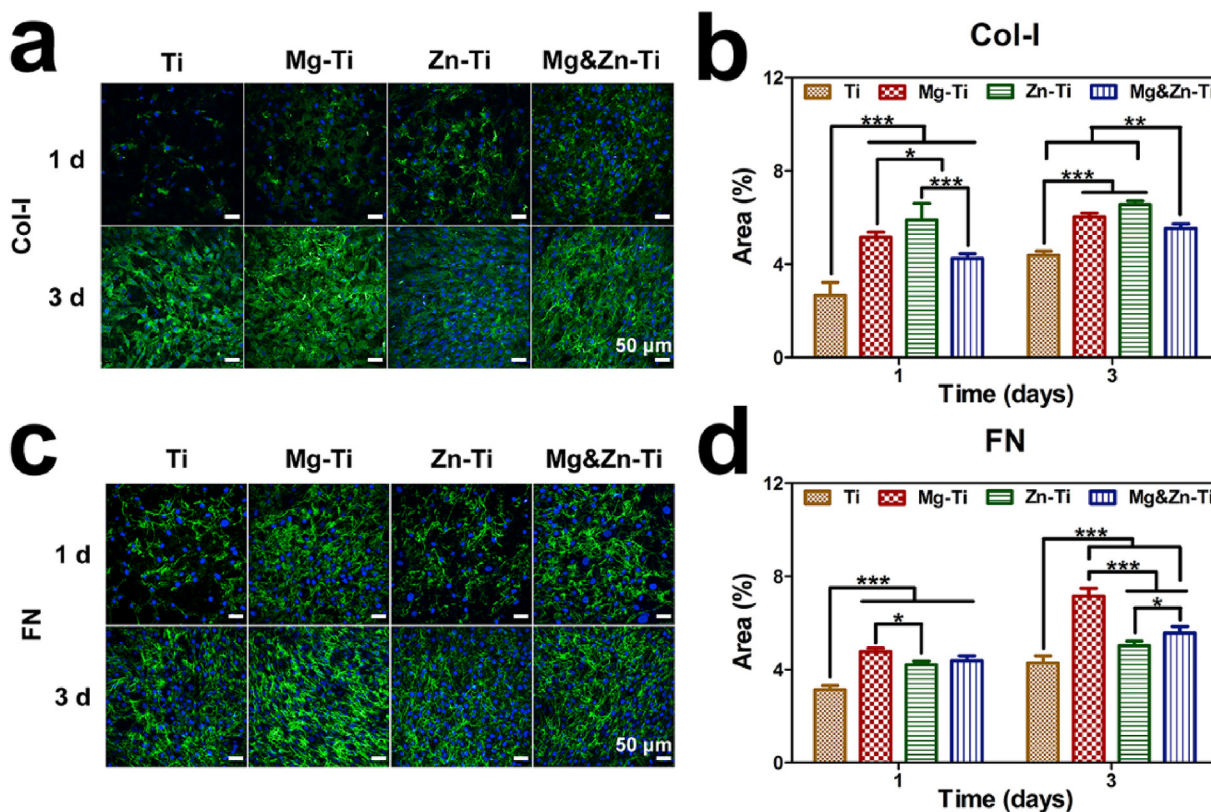

Fig. 5. Immunofluorescence photographs of Col-I (green) obtained by CLSM (a); Semi-quantitative statistical analysis of the immunofluorescence staining intensity of Col-I (b); Immunofluorescence photographs of FN (green) obtained by CLSM (c); Semi-quantitative statistical analysis of the immunofluorescence staining intensity of FN (d); (*p < 0.05; **p < 0.01; ***p < 0.001).

surfaces through regulating cell behaviors such as cell adhesion and migration [53]. Similarly, fibronectin (FN), an important matrix adhesion protein, can build a connection between collagen network and cytoskeletal microfilaments via transmembrane receptors like integrin [53]. Col-I secretion and FN accumulation of HGFs are crucial during

their initial adhesion and are favorable to establish strong and firm soft tissue sealing between implants and tissues [56,57]. Consequently, specific immunofluorescence staining of Col-I and FN were conducted to investigate whether Mg or Zn ion implantation affected HGFs behaviors through changing the organization of ECM. As shown in Fig. 5a,

the secreted Col-I was mainly distributed around single cell on the first day, and it from each cell converged into a network after 3 days. The semi-quantitative statistical analysis of the immunofluorescence staining intensity reflected Col-I secretion of HGFs to some extent, which was because immunofluorescence staining intensity depended on the abundance of protein partly, and the result was shown in Fig. 5b. The immunofluorescence staining intensity of Col-I on implanted samples was higher than that on Ti samples after 1 and 3 days culturing. It suggested that Col-I secretion of HGFs on samples presented the following trend: Zn-Ti > Mg-Ti > Mg&Zn-Ti > Ti. The result of ions release (Fig. 2b and c) showed that Mg&Zn-Ti released more Mg^{2+} than Mg-Ti but less Zn^{2+} than Zn-Ti whereas the immunofluorescence staining intensity of Col-I on Mg&Zn-Ti was lower than those on both Mg-Ti and Zn-Ti. It indicated that Zn ions could regulate Col-I secretion of HGFs, which may rely on the released ions concentration.

Fig. 5c presented FN accumulation of HGFs on various samples. On the first day, FN was centrally distributed around single cell and formed a clear integrated network after the cells were cultured for 3 days. The semi-quantitative statistical analysis of accumulation of FN showed in Fig. 5d obeyed the trend of Mg-Ti > Mg&Zn-Ti > Zn-Ti > Ti, which meant HGFs cultured on all the ion-implanted samples accumulated more substantial FN than cells on Ti. The immunofluorescence staining intensity of FN from HGFs on Mg-Ti was similar to that on Mg&Zn-Ti on the first day but the difference increased after 3 days. It was probably because Mg&Zn-Ti released Mg^{2+} rapidly on 1 day whereas the ions release process of Mg-Ti was slower and more sustained, which could maintain a certain concentration of Mg^{2+} in the medium. Although Zn-Ti released more Zn^{2+} than Mg&Zn-Ti during the culturing time, there were still tiny differences between them in the accumulation of FN. The result of FN accumulation of HGFs on different samples suggested that Mg^{2+} might play a key role in influencing the FN accumulation of HGFs. From the analysis above, it can be inferred that Mg or Zn ion implantation might regulate the behaviors of HGFs through affecting its organization of ECM such as Col-I and FN, so HGFs on ion-implanted samples showed better adhesion, mobility and proliferation, which were important for soft tissue sealing [58].

3.6. Gene expression of HGFs

To investigate how Mg and Zn ion implantation affected the behaviors of HGFs, RT-PCR was performed to analyze the expression of Col-I, TGF-β, FN, Smad2, ITGB1, Smad3, MAPK3, ZIP7, Erk2 and ZIP13 in HGFs that cultured on different samples for 7 days, and the results were displayed in Fig. 6. The expression of Col-I and FN were upregulated in all the ion-implanted samples, consistent with the result of immunofluorescence analysis of Col-I and FN (Fig. 5). As shown in Fig. 6e, the expression of ITGB1 was enhanced in Mg-Ti and Mg&Zn-Ti compared to Zn-Ti and Ti, which was probably because the interaction between integrin and ECM required the participation of divalent ions such as Mg^{2+} or Ca^{2+} [58]. The released Mg^{2+} from Mg ion-implanted and co-implanted samples to the medium would spur the synthesis of integrin when HGFs were cultured on them. Moreover, the expression of TGF-β, which simulated the formation of granulation tissue and secretion of collagen, was simulated in HGFs cultured on all ion-implanted samples, especially for Zn-Ti [59]. Smad2 and Smad3 were highly expressed in HGFs from Zn-Ti, indicating higher proliferation rate of HGFs on Zn-Ti than other groups, agreeing with the result of cell proliferation (Fig. 4b). ZIP13 and ZIP7 expression were both upregulated in cells on Zn-Ti, which indicated that the influx of released Zn^{2+} from extracellular environment and intracellular stores was promoted [60]. However, the expression of ZIP13 was also enhanced in cells cultured on Mg-Ti, which may be ascribed to the probable link between Mg^{2+} and ZIP13, as Fukada et al. reported [61]. The expression of MAPK3 that influenced cell growth and inflammation were slightly upregulated in HGFs seeded on Zn-Ti and Mg&Zn-Ti (Fig. 6g). In addition, it was probably because that Mg ions involved in the function of Erk2 on the

process of protein phosphorylation, Erk2, which played a critical role in cell proliferation and construction of cytoskeleton, exhibited higher expression in HGFs on Mg-Ti than Zn-Ti as shown in Fig. 6i [62,63].

3.7. Regulatory mechanism on the behaviors of HGFs

Through the analysis of RT-PCR and other *in vitro* experiments, we found that Mg and Zn ions could regulate the behaviors of HGFs and thus Mg or Zn ions implantation may have great potential in improving the soft tissue sealing ability of Ti implants. Specifically, HGFs on Mg ion-implanted samples exhibited better adhesion and migration ability than pure Ti and Zn ion-implanted samples. Cell behaviors such as cell adhesion and migration highly relied on integrin receptors, a family of transmembrane glycoproteins that regulated the mutual recognition and adhesion between cells and ECM through connecting the external environment and the internal structure of cells [53,58]. The high expression level of ITGB1 in HGFs on Mg-Ti and Mg&Zn-Ti but relatively lower expression of it on Zn-Ti suggested that Mg^{2+} mainly regulated the motility and adhesion of HGFs by stimulating the expression of ITGB1. Wang et al. and Zhu et al. confirmed that ITGB1 regulated cell motility and adhesion via activating FAK and further triggering downstream biochemical signals [53,64]. The expression of Erk2 in HGFs on Mg-Ti was enhanced, which agreed with the works by Waas et al. that Mg ions were essential to activate Erk2 [63]. Therefore, as shown in Fig. 7a, Mg^{2+} may regulate the motility and adhesion of HGFs through influencing the expression and function of Erk2 and activating MAPK signal pathway. Moreover, many ligands of integrin such as Col-I and FN would tend to combine with integrin and thus deposited on the sample surfaces. They were important compositions of ECM and had significant effects on cell adhesion, migration and spreading. Furthermore, they played key roles in soft tissue sealing through establishing collagen networks [53]. Therefore, thanks to the higher expression level of integrin and substantial accumulation of ECM stimulated by released Mg^{2+}, Mg ion implantation can be an effective method to build a favorable microenvironment around the sample surface for protein adsorption, initial adhesion and migration of HGFs.

On the other hand, HGFs cultured on Zn-Ti had the highest proliferation rate and amount among all groups. Since Smad2 and Smad3 were closely related to cell proliferation, the relatively higher expression of them in HGFs on Zn-Ti than other groups, especially Mg&Zn-Ti whose Zn^{2+} release was lower than Zn-Ti, indicated that Zn^{2+} might be a main reason in regulating HGFs proliferation [65,66]. It was reported that the function and homeostasis of Zn in cells or organisms were mainly controlled by Zn transporters [67,68]. Among all Zn transporters, ZIP13 and ZIP7 were important for soft tissue such as skin development and connective tissue formation [68]. In this work, the expression of ZIP7 and ZIP13 were upregulated in HGFs cultured on Zn-Ti due to the localized high concentration of Zn^{2+} around the surface of Zn-Ti caused by ions release. Fukada et al. and Bin et al. reported ZIP13 involved in the connective tissue development by activating TGF-β signal pathway and influencing the deposition of Col-I, consistent with the results of RT-PCR and immunofluorescence staining in this work that the TGF-β expressed and Col-I secreted in HGFs on Zn-Ti obviously higher than other groups [60,69]. Wen et al. also reported that TGF-β also functioned in fibroblasts by activating MAPK signal pathway including MAPK3 (p38MAPK) through non-canonical way, which was consistent with the slightly enhance expression of MAPK3 in HGFs on Zn-Ti [70]. Considering all the analysis above, the possible involved signal pathways caused by Zn^{2+} were shown in Fig. 7b. When HGFs were cultured on Zn ion-implanted samples, the released Zn^{2+} would spur the expression of ZIP13 and ZIP7 in HGFs to maintain the homeostasis of Zn in cells. The high expression of ZIP13 then stimulated TGF-β and MAPK signal pathways by canonical and non-canonical ways, respectively. Because the activation of TGF-β and MAPK signal pathways, the SMAD family members were triggered and the cell proliferation, protein phosphorylation and ECM accumulation were
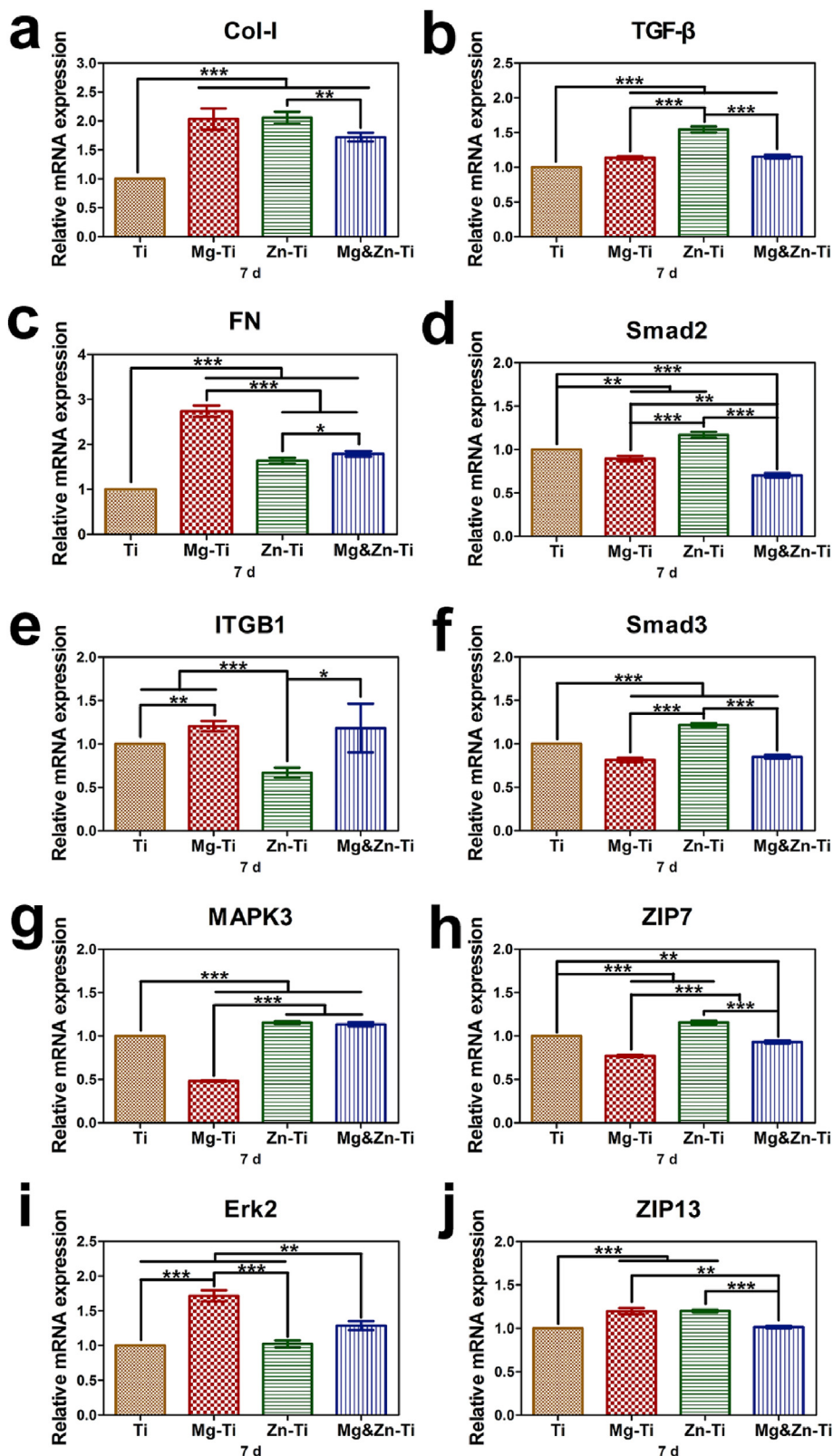
Fig. 6. RT-PCR analysis of gene expression in HGFs cultured on various samples for 7 days: (a) Col-I, (b) TGF-β, (c) FN, (d) Smad2, (e) ITGB1, (f) Smad3, (g) MAPK3, (h) ZIP7, (i) Erk2, (j) ZIP13; (*$p < 0.05$; **$p < 0.01$; ***$p < 0.001$).
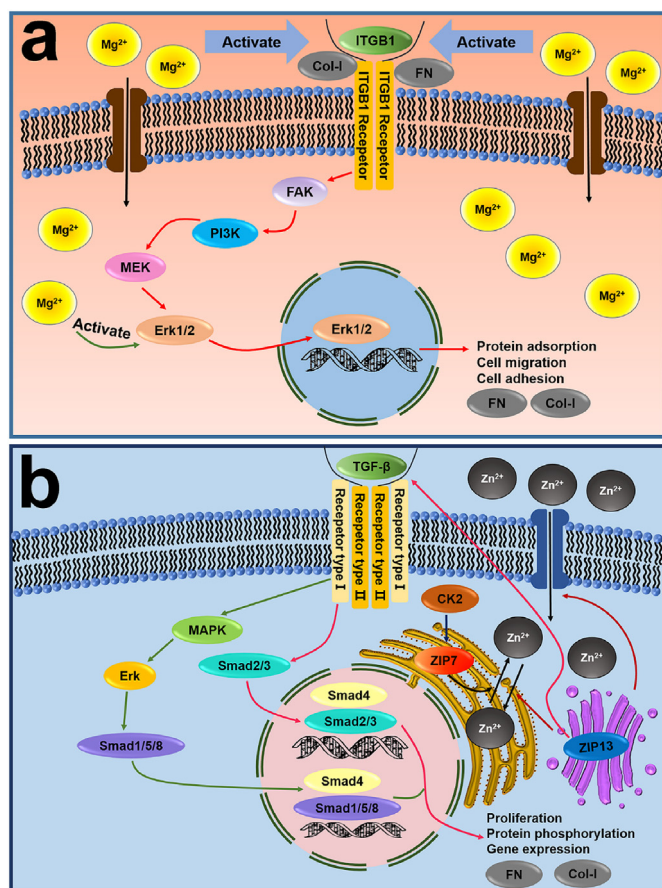
Fig. 7. Illustration for the possible signal pathways of the effects of Mg (a) and Zn (b) ions on the behaviors of HGFs.

promoted.

4. Conclusion

In the present work, Mg and Zn ions implantation were used to improve the soft tissue sealing ability of Ti. The surface wettability of titanium changed after ions implantation, which affected the protein adsorption of sample surfaces. The characterization of physicochemical and biological properties of ion-implanted samples indicated that both Mg and Zn ions can promote the accumulation of ECM such as Col-I and FN. Specifically, Mg^{2+} released from Mg ion-implanted samples led to better adhesion and motility of HGFs probably through regulating the expression of ITGB1 and activating MAPK signal pathway. Released Zn^{2+} caused by Zn ion implantation mainly improved the HGFs proliferation, which can be attributed to the upregulation of ZIP7 and ZIP13 expression as well as the activation of TGF-β signal pathway. The synergistic effect of Mg and Zn ions can endow HGFs cultured on the co-implanted samples with improved cell adhesion, migration and proliferation. The initial adhesion, migration and proliferation of HGFs are key steps during the process of soft tissue sealing. Therefore, Mg and Zn co-implantation is probably a promising way to improve the integration between soft tissue and Ti implants.

CRediT authorship contribution statement

Lanyu Wang: Investigation, Methodology, Formal analysis, Writing - original draft. **Qiming Luo:** Methodology, Validation. **Xianming Zhang:** Methodology, Validation. **Jiajun Qiu:** Writing - review & editing, Validation. **Shi Qian:** Methodology, Project administration, Supervision, Writing - review & editing. **Xuanyong Liu:** Resources,

Conceptualization, Project administration, Writing - review & editing.

Declaration of competing interest

The authors declare that they have no known competing financial interests or personal relationships that could have appeared to influence the work reported in this paper.

Acknowledgment

References

[1] W.S.W. Harun, R.I.M. Asri, J. Alias, F.H. Zulkifli, K. Kadirgama, S.A.C. Ghani, J.H.M. Shariffuddin, A comprehensive review of hydroxyapatite-based coatings adhesion on metallic biomaterials, Ceram. Int. 44 (2018) 1250–1268, https://doi.org/10.1016/j.ceramint.2017.10.162.

[2] C. Domínguez-Trujillo, E. Peón, E. Chicardi, H. Pérez, J.A. Rodríguez-Ortiz, J.J. Pavón, J. García-Couce, J.C. Galván, F. García-Moreno, Y. Torres, Sol-gel deposition of hydroxyapatite coatings on porous titanium for biomedical applications, Surf. Coating. Technol. 333 (2018) 158–162, https://doi.org/10.1016/j.surfcoat.2017.10.079.

[3] A. Ataee, Y. Li, D. Fraser, G. Song, C. Wen, Anisotropic Ti-6Al-4V gyroid scaffolds manufactured by electron beam melting (EBM) for bone implant applications, Mater. Des. 137 (2018) 345–354, https://doi.org/10.1016/j.matdes.2017.10.040.

[4] S. Spriano, S. Yamaguchi, F. Baino, S. Ferraris, A critical review of multifunctional titanium surfaces: new frontiers for improving osseointegration and host response, avoiding bacteria contamination, Acta Biomater. 79 (2018) 1–22, https://doi.org/10.1016/j.actbio.2018.08.013.

[5] F. Rupp, L. Liang, J. Geis-Gerstorfer, L. Scheideler, F. Huttig, Surface characteristics of dental implants: a review, Dent. Mater. 34 (2018) 40–57, https://doi.org/10.1016/j.dental.2017.09.007.

[6] M. Esposito, J.-M. Hirsch, U. Lekholm, P. Thomsen, Biological factors contributing to failures of osseointegrated oral implants (II), Etiopathogenesis, Eur. J. Oral Sci. 106 (1998) 721–764, https://doi.org/10.1046/j.0909-8836.t01-6-.x.

[7] M.N. Abdallah, G. Abughanam, S.D. Tran, Z. Sheikh, M.A. Mezour, T. Basiri, Y. Xiao, M. Cerruti, W.L. Siqueira, F. Tamimi, Comparative adsorption profiles of basal lamina proteome and gingival cells onto dental and titanium surfaces, Acta Biomater. 73 (2018) 547–558, https://doi.org/10.1016/j.actbio.2018.04.017.

[8] A. Besinis, S.D. Hadi, H.R. Le, C. Tredwin, R.D. Handy, Antibacterial activity and biofilm inhibition by surface modified titanium alloy medical implants following application of silver, titanium dioxide and hydroxyapatite nanocoatings, Nanotoxicology 11 (2017) 327–338, https://doi.org/10.1080/17435390.2017.1299890.

[9] F.S.L. Bobbert, K. Lietaert, A.A. Eftekhari, B. Pouran, S.M. Ahmadi, H. Weinans, A.A. Zadpoor, Additively manufactured metallic porous biomaterials based on minimal surfaces: a unique combination of topological, mechanical, and mass transport properties, Acta Biomater. 53 (2017) 572–584, https://doi.org/10.1016/j.actbio.2017.02.024.

[10] A. Civantos, E. Martínez-Campos, V. Ramos, C. Elvira, A. Gallardo, A. Abarrategi, Titanium coatings and surface modifications: toward clinically useful bioactive implants, ACS Biomater. Sci. Eng. 3 (2017) 1245–1261, https://doi.org/10.1021/acsbiomaterials.6b00604.

[11] R. Trindade, T. Albrektsson, S. Galli, Z. Prgomet, P. Tengvall, A. Wennerberg, Osseointegration and foreign body reaction: titanium implants activate the immune system and suppress bone resorption during the first 4 weeks after implantation, Clin. Implant Dent. Relat. Res. 20 (2018) 82–91, https://doi.org/10.1111/cid.12578.

[12] B. Nie, H. Ao, J. Zhou, T. Tang, B. Yue, Biofunctionalization of titanium with bacitracin immobilization shows potential for anti-bacteria, osteogenesis and reduction of macrophage inflammation, Colloids Surf., B 145 (2016) 728–739, https://doi.org/10.1016/j.colsurfb.2016.05.089.

[13] Y. Wang, Y. Zhang, R.J. Miron, Health, Maintenance, and recovery of soft tissues around implants, Clin. Implant Dent. Relat. Res. 18 (2016) 618–634, https://doi.org/10.1111/cid.12343.

[14] M. Chimutengwende-Gordon, R. Dowling, C. Pendegrass, G. Blunn, Determining the porous structure for optimal soft-tissue ingrowth: an in vivo histological study, PloS One 13 (2018) e0206228, , https://doi.org/10.1371/journal.pone.0206228.

[15] Y. Zhao, H. Cao, H. Qin, T. Cheng, S. Qian, M. Cheng, X. Peng, J. Wang, Y. Zhang, G. Jin, X. Zhang, X. Liu, P.K. Chu, Balancing the osteogenic and antibacterial properties of titanium by codoping of Mg and Ag: an in vitro and in vivo study, ACS Appl. Mater. Interfaces 7 (2015) 17826–17836, https://doi.org/10.1021/acsami.5b04168.

[16] X. Rodriguez, A. Navajas, X. Vela, A. Fortuno, J. Jimenez, M. Nevins, Arrangement

of peri-implant connective tissue fibers around platform-switching implants with conical abutments and its relationship to the underlying bone: a human histologic study, Int. J. Periodontics Restor. Dent. 36 (2016) 533–540, https://doi.org/10.11607/prd.2580.

[17] P.R. Klokkevold, Soft Tissue Management for Implants in the Aesthetic Zone, Springer, Los Angeles, 2019.

[18] R. Glauser, P. Schüpbach, J. Gottlow, C.H.F. Hämmerle, Periimplant soft tissue barrier at experimental one-piece mini-implants with different surface topography in humans: a light-microscopic overview and histometric analysis, Clin. Implant Dent. Relat. Res. 7 (2005) S44–S51, https://doi.org/10.1111/j.1708-8208.2005.tb00074.x.

[19] I. Atsuta, Y. Ayukawa, R. Kondo, W. Oshiro, Y. Matsuura, A. Furuhashi, Y. Tsukiyama, K. Koyano, Soft tissue sealing around dental implants based on histological interpretation, J. Prosthodon. Res. 60 (2016) 3–11, https://doi.org/10.1016/j.jpor.2015.07.001.

[20] S. Ivanovski, R. Lee, Comparison of peri-implant and periodontal marginal soft tissues in health and disease, Periodontol (2000) 1–15, https://doi.org/10.1111/prd.12150 0 (2017).

[21] M. Chen, L. Li, Z. Wang, P. Li, F. Feng, X. Zheng, High molecular weight hyaluronic acid regulates P. gingivalis-induced inflammation and migration in human gingival fibroblasts via MAPK and NF-kappaB signaling pathway, Arch. Oral Biol. 98 (2019) 75–80, https://doi.org/10.1016/j.archoralbio.2018.10.027.

[22] X. Wang, Y. Zhang, J. Choukroun, S. Ghanaati, R.J. Miron, Behavior of gingival fibroblasts on titanium implant surfaces in combination with either injectable-PRF or PRP, Int. J. Mol. Sci. 18 (2017) 331, https://doi.org/10.3390/ijms18020331.

[23] T. Abe, Y. Abe, Y. Aida, Y. Hara, K. Maeda, Extracellular matrix regulates induction of alkaline phosphatase expression by ascorbic acid in human fibroblasts, J. Cell. Physiol. 189 (2001) 144–151, https://doi.org/10.1002/jcp.10011.

[24] S. Ellinger, Nutritional Supplements for Critically Ill Patients: Efficient Tools to Improve Wound Healing, Springer, New York, 2015.

[25] R. Razzaghi, F. Pidar, M. Momen-Heravi, F. Bahmani, H. Akbari, Z. Asemi, Magnesium supplementation and the effects on wound healing and metabolic status in patients with diabetic foot ulcer: a randomized, double-blind, placebo-controlled trial, Biol. Trace Elem. Res. 181 (2018) 207–215, https://doi.org/10.1007/s12011-017-1056-5.

[26] X.H. Wang, J.S. Ni, N.L. Cao, S. Yu, Y.G. Chen, S.X. Zhang, B.J. Gu, J. Yan, In Vivo evaluation of Mg-6Zn and titanium alloys on collagen metabolism in the healing of intestinal anastomosis, Sci. Rep. 7 (2017) 44919, https://doi.org/10.1038/srep44919.

[27] K. Rokosz, T. Hryniewicz, S. Gaiaschi, P. Chapon, S. Raaen, D. Matysek, L. Dudek, K. Pietrzak, Novel porous Phosphorus(-)Calcium(-)Magnesium coatings on titanium with copper or zinc obtained by DC plasma electrolytic oxidation: fabrication and characterization, Materials 11 (2018), https://doi.org/10.3390/ma11091680.

[28] Y. Yu, G. Jin, Y. Xue, D. Wang, X. Liu, J. Sun, Multifunctions of dual Zn/Mg ion co-implanted titanium on osteogenesis, angiogenesis and bacteria inhibition for dental implants, Acta Biomater. 49 (2017) 590–603, https://doi.org/10.1016/j.actbio.2016.11.067.

[29] B.S. Kim, J.S. Kim, Y.M. Park, B.Y. Choi, J. Lee, Mg ion implantation on SLA-treated titanium surface and its effects on the behavior of mesenchymal stem cell, Mater. Sci. Eng. C 33 (2013) 1554–1560, https://doi.org/10.1016/j.msec.2012.12.061.

[30] G. Jin, H. Qin, H. Cao, Y. Qiao, Y. Zhao, X. Peng, X. Zhang, X. Liu, P.K. Chu, Zn/Ag micro-galvanic couples formed on titanium and osseointegration effects in the presence of S. aureus, Biomaterials 65 (2015) 22–31, https://doi.org/10.1016/j.biomaterials.2015.06.040.

[31] G. Jin, H. Qin, H. Cao, S. Qian, Y. Zhao, X. Peng, X. Zhang, X. Liu, P.K. Chu, Synergistic effects of dual Zn/Ag ion implantation in osteogenic activity and anti-bacterial ability of titanium, Biomaterials 35 (2014) 7699–7713, https://doi.org/10.1016/j.biomaterials.2014.05.074.

[32] H. Okawachi, Y. Ayukawa, I. Atsuta, A. Furuhashi, M. Sakaguchi, K. Yamane, K. Koyano, Effect of titanium surface calcium and magnesium on adhesive activity of epithelial-like cells and fibroblasts, Biointerphases 7 (2012) 27, https://doi.org/10.1007/s13758-012-0027-9.

[33] Y. Sasaki, G.A. Sathi, O. Yamamoto, In vivo evaluation of wound healing property of zinc smectite using a rat model, J. Ceram. Soc. Jpn. 124 (2016) 1199–1204, https://doi.org/10.2109/jcersj2.16153.

[34] S. Chen, L. Tan, B. Zhang, Y. Xia, K. Xu, K. Yang, In Vivo study on degradation behavior and histologic response of pure magnesium in muscles, J. Mater. Sci. Technol. 33 (2017) 469–474, https://doi.org/10.1016/j.jmst.2016.09.011.

[35] H. Liao, Y. Chen, S. Jeng, Association of zinc with connective tissue in the digestive tract of common carp, Fish. Sci. 72 (2006) 893–902, https://doi.org/10.1111/j.1444-2906.2006.01233.x.

[36] L. Zhang, J. Guo, T. Yan, Y. Han, Fibroblast responses and antibacterial activity of Cu and Zn co-doped TiO2 for percutaneous implants, Appl. Surf. Sci. 434 (2018) 633–642, https://doi.org/10.1016/j.apsusc.2017.10.169.

[37] C. Xia, D. Cai, J. Tan, K. Li, Y. Qiao, X. Liu, Synergistic effects of N/Cu dual ions implantation on stimulating antibacterial ability and angiogenic activity of titanium, ACS Biomater. Sci. Eng. 4 (2018) 3185–3193, https://doi.org/10.1021/acsbiomaterials.8b00501.

[38] L. Wang, J. Qiu, J. Guo, D. Wang, S. Qian, H. Cao, X. Liu, Regulating the behavior of human gingival fibroblasts by sp^2 domains in reduced graphene oxide, ACS Biomater. Sci. Eng. 5 (2019) 6414–6424, https://doi.org/10.1021/acsbiomaterials.9b00497.

[39] B. Hinz, Matrix mechanics and regulation of the fibroblast phenotype, Periodontol 63 (2000) 14–28, https://doi.org/10.1111/prd.12030 2013.

[40] G. Hillmann, A. Gebert, W. Geurtsen, Matrix expression and proliferation of primary gingival fibroblasts in a threedimensional cell culture model, J. Cell Sci. 112 (1999)

[41] L. Jiao, Y. Zhou, P. Hou, Cross section for single ionization of magnesium by electron impact, Phys. Lett. 372 (2008) 5318–5320, https://doi.org/10.1016/j.physleta.2008.06.034.

[42] X. Feng, L. Feng, M. Jin, J. Zhai, L. Jiang, D. Zhu, Reversible super-hydrophobicity to super-hydrophilicity transition of aligned ZnO nanorod films, J. Am. Chem. Soc. 126 (2004) 62–63, https://doi.org/10.1021/ja038636o.

[43] J. Lv, C. Liu, F. Wang, Z. Zhou, Z. Zi, Y. Feng, X. Chen, F. Liu, G. He, S. Shi, X. Song, Z. Sun, Influence of solution concentrations on surface morphology and wettability of ZnO thin films, Electron. Mater. Lett. 9 (2013) 171–176, https://doi.org/10.1007/s13391-012-2170-3.

[44] J. Wang, D. Li, Q. Liu, X. Yin, Y. Zhang, X. Jing, M. Zhang, Fabrication of hydrophobic surface with hierarchical structure on Mg alloy and its corrosion resistance, Electrochim. Acta 55 (2010) 6897–6906, https://doi.org/10.1016/j.electacta.2010.05.070.

[45] G. Ning, Y. Liu, F. Wei, Q. Wen, G. Luo, Porous and lamella-like Fe/MgO catalysts prepared under hydrothermal conditions for high-yield synthesis of double-walled carbon nanotubes, J. Phys. Chem. C 111 (2007) 1969–1975, https://doi.org/10.1021/jp064483q.

[46] M.S. Antelman, F.J. Harris, The Encyclopedia of Chemical Electrode Potentials, Springer, Boston, 1982.

[47] M. Ferrari, F. Cirisano, M.C. Morán, Mammalian cell behavior on hydrophobic substrates: influence of surface properties, Colloids Interfaces 3 (2019) 48, https://doi.org/10.3390/colloids3020048.

[48] B. Koley Seth, A. Ray, M. Banerjee, T. Bhattacharyya, D. Bhattacharyya, S. Basu, Structure dependent hydrophobic and hydrophilic interactions between nickel(II) Schiff base complexes and serum albumins: spectroscopic and docking studies, J. Lumin. 171 (2016) 85–97, https://doi.org/10.1016/j.jlumin.2015.11.009.

[49] Y.L. Jeyachandran, E. Mielczarski, B. Rai, J.A. Mielczarski, Quantitative and qualitative evaluation of adsorption/desorption of bovine serum albumin on hydrophilic and hydrophobic surfaces, Langmuir 25 (2009) 11614–11620, https://doi.org/10.1021/la901453a.

[50] J. Wei, T. Igarashi, N. Okumori, T. Igarashi, T. Maetani, B. Liu, M. Yoshinari, Influence of surface wettability on competitive protein adsorption and initial attachment of osteoblasts, Biomed. Mater. 4 (2009) 045002, , https://doi.org/10.1088/1748-6041/4/4/045002.

[51] J.R.W. Conway, G. Jacquemet, Cell matrix adhesion in cell migration, Essays Biochem. 63 (2019) 535–551, https://doi.org/10.1042/EBC20190012.

[52] R. Aguilar-Cuenca, C. Llorente-Gonzalez, C. Vicente, M. Vicente-Manzanares, Microfilament-coordinated adhesion dynamics drives single cell migration and shapes whole tissues, F1000Research 6 (2017) 160, https://doi.org/10.12688/f1000research.10356.1.

[53] X. Wang, T. Lu, J. Wen, L. Xu, D. Zeng, Q. Wu, L. Cao, S. Lin, X. Liu, X. Jiang, Selective responses of human gingival fibroblasts and bacteria on carbon fiber reinforced polyetheretherketone with multilevel nanostructured TiO2, Biomaterials 83 (2016) 207–218, https://doi.org/10.1016/j.biomaterials.2016.01.001.

[54] T. Xia, M. Kovochich, M. Liong, L. Madler, B. Gilbert, H. Shi, J.I. Yeh, J.I. Zink, A.E. Nel, Comparison of the mechanism of toxicity of zinc oxide and cerium oxide nanoparticles based on dissolution and oxidative stress properties, ACS Nano 2 (2008) 2121–2134, https://doi.org/10.1021/nn800511k.

[55] H. Yang, C. Liu, D. Yang, H. Zhang, Z. Xi, Comparative study of cytotoxicity, oxidative stress and genotoxicity induced by four typical nanomaterials: the role of particle size, shape and composition, J. Appl. Toxicol. 29 (2009) 69–78, https://doi.org/10.1002/jat.1385.

[56] M.B. Asparuhova, D. Kiryak, M. Eliezer, D. Mihov, A. Sculean, Activity of two hyaluronan preparations on primary human oral fibroblasts, J. Periodontal. Res. 54 (2019) 33–45, https://doi.org/10.1111/jre.12602.

[57] C.M. Stanley, Y. Wang, S. Pal, R.J. Klebe, L.B. Harkless, X. Xu, Z. Chen, B. Steffensen, Fibronectin fragmentation is a feature of periodontal disease sites and diabetic foot and leg wounds and modifies cell behavior, J. Periodontol. 79 (2008) 861–875, https://doi.org/10.1902/jop.2008.070492.

[58] T.S. Lange, K. Kirchberg, A.K. Bielinsky, A. Leuker, I. Bank, T. Ruzicka, K. Scharftetter-Kochanek, Divalent cations (Mg^{2+}, Ca^{2+}) differentially influence the Pi integrin-mediated migration of human fibroblasts and keratinocytes to different extracellular matrix proteins, Exp. Dermatol. 4 (1995) 130–137, https://doi.org/10.1111/j.1600-0625.1995.tb00236.x.

[59] L. Nan, Y. Zheng, N. Liao, S. Li, Y. Wang, Z. Chen, L. Wei, S. Zhao, S. Mo, Mechanical force promotes the proliferation and extracellular matrix synthesis of human gingival fibroblasts cultured on 3D PLGA scaffolds via TGFbeta expression, Mol. Med. Rep. 19 (2019) 2107–2114, https://doi.org/10.3892/mmr.2019.9882.

[60] B.H. Bin, J. Bhin, J. Seo, S.Y. Kim, E. Lee, K. Park, D.H. Choi, T. Takagishi, T. Hara, D. Hwang, H. Koseki, Y. Asada, S. Shimoda, K. Mishima, T. Fukada, Requirement of zinc transporter SLC39A7/ZIP7 for dermal development to fine-tune endoplasmic reticulum function by regulating protein disulfide isomerase, J. Invest. Dermatol. 137 (2017) 1682–1691, https://doi.org/10.1016/j.jid.2017.03.031.

[61] T. Fukada, Y. Asada, K. Mishima, S. Shimoda, I. Saito, Slc39a13/Zip13: a crucial zinc transporter involved in tooth development and inherited disorders, J. Oral Biosci. 53 (2011) 1–12, https://doi.org/10.2330/joralbiosci.53.1.

[62] T.S. Kaoud, A.K. Devkota, R. Harris, M.S. Rana, O. Abramczyk, M. Warthaka, S. Lee, M.E. Girvin, A.F. Riggs, K.N. Dalby, Activated ERK2 is a monomer in vitro with or without divalent cations and when complexed to the cytoplasmic scaffold PEA-15, Biochemistry 50 (2011) 4568–4578, https://doi.org/10.1021/bi200202y.

[63] W.F. Waas, K.N. Dalby, Physiological concentrations of divalent magnesium ion activate the serine/threonine specific protein kinase ERK2, Biochemistry 42 (2003) 2960–2970, https://doi.org/10.1021/bi027171w.

[64] Y. Zhu, C.N. Zhang, Y.X. Gu, J.Y. Shi, J.J. Mo, S.J. Qian, S.C. Qiao, H.C. Lai, The

responses of human gingival fibroblasts to magnesium-doped titanium, J. Biomed. Mater. Res. 108 (2020) 267–278, https://doi.org/10.1002/jbm.a.36813.

[65] N. Tandon, E. Cimetta, A. Villasante, N. Kupferstein, M.D. Southall, A. Fassih, J. Xie, Y. Sun, G. Vunjak-Novakovic, Galvanic microparticles increase migration of human dermal fibroblasts in a wound-healing model via reactive oxygen species pathway, Exp. Cell Res. 320 (2014) 79–91, https://doi.org/10.1016/j.yexcr.2013.09.016.

[66] L. Liu, Y. Pan, C. Zhai, Y. Zhu, R. Ke, W. Shi, J. Wang, X. Yan, X. Su, Y. Song, L. Gao, M. Li, Activation of peroxisome proliferation-activated receptor-gamma inhibits transforming growth factor-beta1-induced airway smooth muscle cell proliferation by suppressing Smad-miR-21 signaling, J. Cell. Physiol. 234 (2018) 669–681, https://doi.org/10.1002/jcp.26839.

[67] T. Kambe, An overview of a wide range of functions of ZnT and Zip zinc transporters in the secretory pathway, Biosci. Biotechnol. Biochem. 75 (2011) 1036–1043, https://doi.org/10.1271/bbb.110056.

[68] N. Levaot, M. Hershfinkel, How cellular Zn(2+) signaling drives physiological functions, Cell Calcium 75 (2018) 53–63, https://doi.org/10.1016/j.ceca.2018.08.004.

[69] T. Fukada, N. Civic, T. Furuichi, S. Shimoda, K. Mishima, H. Higashiyama, Y. Idaira, Y. Asada, H. Kitamura, S. Yamasaki, S. Hojyo, M. Nakayama, O. Ohara, H. Koseki, H.G. dos Santos, L. Bonafe, R. Ha-Vinh, A. Zankl, S. Unger, M.E. Kraenzlin, J.S. Beckmann, I. Saito, C. Rivolta, S. Ikegawa, A. Superti-Furga, T. Hirano, The zinc transporter SLC39A13/ZIP13 is required for connective tissue development; its involvement in BMP/TGF-b signaling pathways, PloS One 3 (2008) e3642, , https://doi.org/10.1371/journal.pone.0003642.

[70] J. Wen, X. Lin, W. Gao, B. Qu, Y. Ling, R. Liu, M. Yu, MEK inhibition prevents TGFbeta1induced myofibroblast transdifferentiation in human tenon fibroblasts, Mol. Med. Rep. 19 (2019) 468–476, https://doi.org/10.3892/mmr.2018.9673.